Hindawi
Wireless Communications and Mobile Computing
Volume 2023, Article ID 1538872, 13 pages
https://doi.org/10.1155/2023/1538872

*Research Article*

# Gain of Spatial Diversity with Conjoint Signals in Arbitrarily Correlated Rayleigh Fading Channels

**Edwin Omosa**,[1] **Peter Akuon**,[1] **Hongjun Xu**,[2] **and Vitalis Oduol**[1]

[1]*School of Engineering, University of Nairobi, P O Box 30197-00100, Nairobi, Kenya*
[2]*School of Engineering, University of KwaZulu-Natal, Durban 4041, South Africa*

Correspondence should be addressed to Edwin Omosa; edwinomosa@gmail.com

Received 28 March 2023; Revised 2 October 2023; Accepted 25 October 2023; Published 21 November 2023

Academic Editor: Sujan Rajbhandari



Coding gains for arbitrarily correlated signals in a spatial diversity system with conjoint signals are presented in this study. The basic form of the proposed signal synthesizer evenly produces phase changes in the output signals. The mixer is an orthogonal transformation matrix, which is energy preserving and blind to the channel correlation matrix. The idea is to synthesize additional conjoint signal copies from the received signals that would be received if there were more antennas. However, these conjoint signals contain a level of correlation with the received signals. With the assumption of flat Rayleigh fading channels, simulation results for symbol error probability (SEP) are presented for different numbers of receive branches and varying correlation conditions. It is shown that under binary phase shift keying (BPSK), the synthesizer achieves decorrelation coding gains of about 1 dB when selection combining (SC) or equal gain combining (EGC) is used. The synthesizer's performance across M-ary quadrature amplitude modulation (MQAM) signals is also tested. In addition, analytical frameworks are derived for BPSK and MQAM, which are tightly bound by the Monte Carlo simulation results obtained using Matlab. The correlation analysis is performed for different numbers of antennas and varied antenna spacings.

## 1. Introduction

Receive diversity approaches are recognized to increase numerous figures of merit in wireless communications systems by providing redundant signals that can be combined to achieve a better quality of service (QoS) [1–8]. However, space restrictions, e.g., in mobile handsets make it difficult to receive uncorrelated signals, hence the need for decorrelation [3, 9–11]. In fact, several instantaneous decorrelation algorithms are known, but signal information measurements are required.

Also, blind decorrelation schemes or virtual antennas, e.g., discrete Fourier transform (DFT) do not measure signal information, but they require uniform circular receive antenna spacing configurations [12–14]. Furthermore, the state-of-the-art decorrelation algorithms in open literature are not unifying when different signal combining techniques are used to combine the decorrelated output signals [15–21].

For example, Hangani and Beaulieu [21] showed how intuitive decorrelation of signals for dual branch systems can be achieved through eigenvalue decomposition (EVD) of the received signals. The low-complexity dual decorrelator, which was formerly presented in a study by Fang et al. [19], does not assume the knowledge of the correlation matrix and can, therefore, be referred to as a blind decorrelator [12–14]. The blind decorrelator in a study by Hangani and Beaulieu [21] has been used in a study by Hangani and Beaulieu [21] and Dong and Beaulieu [22] to examine decorrelation benefits for various diversity combining techniques. It is observed that for moderate signal-to-noise ratio (SNR) levels, the decorrelator nonuniformly improves performance only for the selection combining (SC) system by redistributing the received signal power among the receive branches [15, 21, 22].

Generally, the dual decorrelator is simple to implement and is suitable for use in error analysis for correlated branches [15, 21, 22]. However, theoretical analysis reveals that the dual decorrelator is always energy preserving, but may lead to signal zeroing since its transformation matrix consists of real entries only [23]. In fact, it is observed that it

is only optimal for maximal ratio combining (MRC) [6, 19, 22, 24, 25], but alters the performance criteria for SC and equal gain combining (EGC) and cannot be used as a unifying decorrelator for dual diversity systems [19, 20, 26–28].

Furthermore, it has been demonstrated in a study by Akuon and Xu [28] that a similar decorrelator as proposed in a study by Akuon and Xu [27] achieves coding gains across SC and EGC combiners under independent flat fading Rayleigh channels. This paper aims to theoretically and experimentally show that coding gains are achieved using conjoint signals even under arbitrarily correlated flat fading Rayleigh channels. In a nonflat Rayleigh fading model, the fading behavior of the channel exhibits variations over frequency or time. This inherent inconsistency implies that the channel's characteristics undergo modifications across various frequency components or the duration of time. This variability presents challenges in communication systems, as it results in fluctuations in signal strength and quality, primarily attributable to signal attenuation and rapid fluctuations in both amplitude and phase. To combat nonflat fading in wireless communication systems, a combination of strategies is essential [29]. These methods address signal strength variations and phase deviations across different frequency ranges. Within this framework, various techniques are encompassed, such as channel equalization, orthogonal frequency division multiplexing (OFDM), adaptive modulation and coding, diversity schemes, hybrid automatic repeat request (ARQ), and frequency hopping spread spectrum (FHSS). Moreover, the transformation of variable channel parameters into uniform values using interpolation or sampling, coupled with the utilization of the rake receiver, constitutes a pivotal aspect of this toolkit. This add extra complexity to the system hence, the preference of flat Rayleigh fading.

In the proposed method, the introduction of supplementary diversity paths, often referred to as excess virtual antennas, becomes accessible as a consequence of the spatial separation among the receiving elements. The power loss stemming from inefficiencies is estimated by postulating that signals lost within the geometric area of an antenna are intercepted by neighboring antennas. The quantification of this power loss involves the generation of conjoint signals, without the need for instantaneous signal strength measurements. These conjoint signals are locally synthesized at the receiver through a process encompassing conjugation, summation, or subtraction of two distinct amplitudes or phases derived from the received signals without any channel state information. This combination yields signals akin to those obtained through real-time measurements, thereby obviating the necessity for instantaneous measurement.

The following are summaries of the contributions in this paper:

(1) It is shown that the proposed signal synthesizer achieves diversity coding gain, which is unifying for both the SC and the EGC schemes for binary phase shift keying (BPSK) and M-ary quadrature amplitude modulation (MQAM) under arbitrary channel correlation.

(2) In addition, it is shown that the proposed decorrelator is blind, thus simple because it does not estimate the correlation matrix, but depends on the coding gains inherent in the conjoint signals, which are arithmetically synthesized from the received signals.

(3) The synthesizer is unifying for SC and EGC even under correlation, it's blind, and doesn't lead to signal zeroing even under correlation.

(4) Validation framework is provided in relation to symbol error probability (SEP) for both BPSK and MQAM. To do so, the SNR at the combiner output and the SNR at the diversity synthesizer output are analyzed and used to evaluate the gain of the overall system. The gain parameter is then applied to the optimal error analysis for correlated systems.

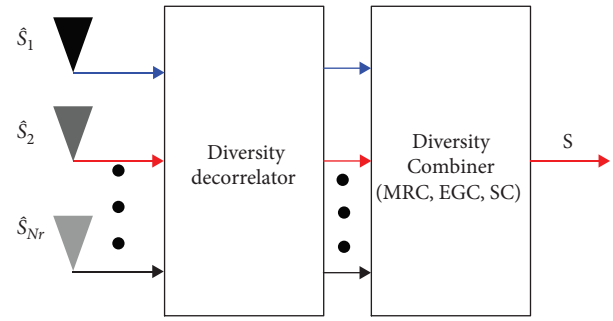


Figure 1: The conjoint diversity model.

The paper is structured as follows: Section 2 introduces the decorrelation system model. In addition, arbitrary correlations are examined. The discussion on the proposed decorrelator is also provided in this section. This is followed by the discussion on the combined output SNR after decorrelation. The system performance is analyzed in Section 3. Then, a comparison of simulation results with theoretical results is done in Section 4. Section 5 brings the work to a close.

In this work, matrices are represented by bold uppercase symbols, while ordinary letters imply scalar quantities. The Gaussian Q-function is denoted by $Q(.)$. Furthermore, the operators $E[.]$, $(.)^*$, and $(.)^H$ signify the expectation, complex conjugate, and Hermitian operators, respectively. Finally, $J_0(\cdot)$ represents the zero-order Bessel function of the first kind.

## 2. Conjoint Diversity System

*2.1. Correlated Signal Model.* We consider a general $N_r$ branch diversity system, as shown in Figure 1. The received branch signals are processed through a diversity decorrelator, which produces an additional array of the received signals. These newly synthesized signals are then processed through the conventional diversity combiner of choice to acquire an approximate of the transmitted symbol. The uncorrelated received signal at the $k_{th}$ branch is expressed as follows:

$$s_k = \alpha_k A_m e^{j\psi_k} e^{j\phi_m} + n_k,\ k = 1, 2, \ldots, N_r, \tag{1}$$

where $A_m$ is the amplitude of the transmitted signal, $\phi_m$ denotes the phase angle of transmitted signal, $\alpha_k$ denotes the Rayleigh distributed random amplitude with $E[\alpha_k^2] = 2\sigma_k^2$, $\psi_k$ denotes a random phase process, and $n_k$ denotes zero-mean Gaussian noise. The noise components are assumed to be uncorrelated with each other and independent of the signals [27]. The dependence on the index $m$ can be removed for symbol-by-symbol detection.

The signal received via correlated Rayleigh fading channel with a correlation coefficient $\rho$ is expressed as follows:

$$\widehat{s}_k = (X_k + Y_k)e^{j\phi_m} + n_k,\ k = 1, 2, \ldots, N_r, \tag{2}$$

where $X_k$ and $Y_k$ are Gaussian random variables with $\mathrm{var}(X_k) = \mathrm{var}(Y_k) = \sigma^2$ and $\mu = 0$. $\mathrm{var}(X_k)$ and $\mu$ are the variance and mean, respectively.

$$E[X_i Y_k] = 0 \quad i, k = 1, 2, \ldots, N, \tag{3}$$

$$C_{X_i X_k} = E[X_i X_k] = \rho\sigma^2, \tag{4}$$

$$C_{Y_i Y_k} = E[Y_i Y_k] = \rho\sigma^2. \tag{5}$$

Similarly, because the noise components are uncorrelated and statistically independent, we can write as follows:

$$E[n_i n_k] = E[n_i X_k] = E[n_i Y_k] = 0. \tag{6}$$

Taking $\rho_{kl}$ as the coefficient of correlation between the $k_{th}$ and $l_{th}$ branches, $\rho_{kl}$ can be expressed as follows [5]:

$$\rho_{kl} = \frac{E\left[\widehat{h}_k \widehat{h}_l^*\right]}{\sqrt{\sigma^2_{\widehat{h}_k}\,\sigma^2_{\widehat{h}_l}}},\ l, k = 1, 2, \ldots, N_r, \tag{7}$$

where $\sigma^2_{\widehat{h}_k}$ represents the variance of the random variables (RV) $\widehat{h}_k$, and $\sigma^2_{\widehat{h}_l}$ is the variance of the RV $\widehat{h}_l$.

If $R$ is a normalized correlation matrix, it can be represented as follows [5, 27]:

$$R = \begin{pmatrix} 1 & \rho_{12} & \cdots & \rho_{1N_r} \\ \rho_{21} & 1 & \cdots & \rho_{2N_r} \\ \vdots & \vdots & \ddots & \vdots \\ \rho_{N_r 1} & \cdots & \cdots & 1 \end{pmatrix}. \tag{8}$$

From the definitions in Equation (7), it is evident that the correlation coefficients $\rho_{k,l}$ and $\rho_{l,k}$ are complex conjugates, that is, $\rho_{k,l} = \rho^*_{l,k}$. Thus, the normalized correlation matrix is Hermitian (equal to its conjugate transpose), $R^H = R$. In a study by Akuon and Xu [28], $R$ is expected to have positive eigenvalues and to be positive definite.

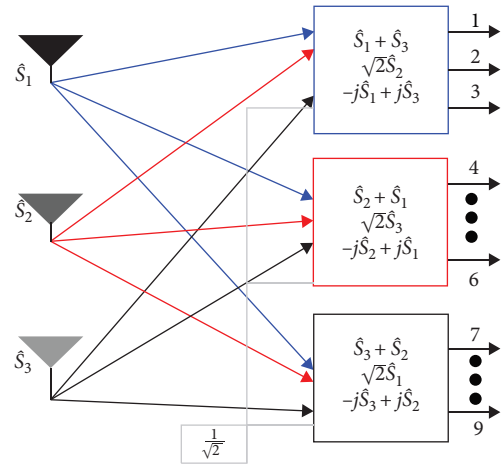


FIGURE 2: Decorrelation synthesizer system with $N_r = 3$ and $\theta = 45^0$.

*2.2. Equivalent Eigen-Filter Signal Model.* EVD may be applied to breakdown $R$ into orthogonal eigenvectors and eigenvalues (EVD). This may be accomplished via an eigen-filter operation, as described in a study by Akuon and Xu [28], Simon and Alouini [29], Xu [30], Zhang et al. [17], de Barros et al. [31], and Pan et al. [33], as follows:

$$\begin{aligned} \Lambda &= QRQ^H, \\ R &= Q^H \Lambda Q, \end{aligned} \tag{9}$$

where $Q$ is the orthonormal eigenvector matrix and $\Lambda$ is the positive eigenvalue matrix. Decomposition through EVD yields $Q$, with rows constituting orthonormal basis elements, making $Q$ a unitary transformation. Further, $Q^H = Q^{-1}$. $Q$ generates a reciprocal network. Hence, $Q$ is the designed eigen-filter/diversity decorrelator that yields an output attributed to unitary input modification. The operation of the filter is well analyzed in a study by Akuon and Xu [28].

*2.3. Basis Signal Synthesizer.* In its simplest form, the proposed diversity decorrelator is a dual transformation matrix, which is given as follows:

$$Q^H = \begin{pmatrix} \cos\theta & \cos\theta \\ -j\sin\theta & j\sin\theta \end{pmatrix}. \tag{10}$$

Let the independent channels have identical amplitudes such that $\theta = 45^0$, and let $z_k$ be the transmitted symbol. For a two-branch system with the inputs $\widehat{s_1}$ and $\widehat{s_2}$, we can use Equation (10) to express the signals at the output of the decorrelator as $\widehat{v} = Q^H \widehat{s}$, which is expressed as follows [27]:

$$\begin{pmatrix} \widehat{v}_3 \\ \widehat{v}_4 \end{pmatrix} = \frac{1}{\sqrt{2}} \begin{pmatrix} 1 & 1 \\ -j & j \end{pmatrix} \begin{pmatrix} \widehat{s_1} \\ \widehat{s_2} \end{pmatrix}. \tag{11}$$

Subsequently, we can expand Equations (11) as (2).

$$\begin{aligned}\widehat{v}_3 &= \frac{1}{\sqrt{2}}(X_1 + jY_1)\widehat{s}_1 + \frac{1}{\sqrt{2}}(X_2 + jY_2)\widehat{s}_2 + \frac{1}{\sqrt{2}}(n_1 + n_2)\\ &= \left(\frac{1}{\sqrt{2}}(X_1 + X_2)\right)\widehat{s}_1 + j\left(\frac{1}{\sqrt{2}}(Y_1 + Y_2)\right)\widehat{s}_2 + \frac{1}{\sqrt{2}}(n_1 + n_2)\\ \widehat{v}_4 &= -j\frac{1}{\sqrt{2}}(X_1 + jY_1)\widehat{s}_1 + j\frac{1}{\sqrt{2}}(X_2 + jY_2)\widehat{s}_2 + \frac{1}{\sqrt{2}}(-jn_1 + jn_2)\\ &= \left(\frac{1}{\sqrt{2}}(Y_1 - Y_2)\right)\widehat{s}_1 + j\left(\frac{1}{\sqrt{2}}(X_2 - X_1)\right)\widehat{s}_2 + \frac{1}{\sqrt{2}}(n_2 - jn_1)\end{aligned}. \tag{12}$$

*2.4. $N_r$ Branch Synthesizer Operation.* In order to effect the blind decorrelation for $N_r$ branches, as shown in Figure 2, the approach entails conducting a specific operation in Equation (12) on each pair of branch signals. This will produce $N_r(N_r - 1)$ decorrelated outputs. Then, we combine the decorrelated signals with the $N_r$ received signals. In total, there will be $N_r^2$ signals at the input of the diversity combiner, as shown in Figure 2.

*2.5. Diversity Combining.* Finally, we perform a diversity combining operation on the $N_r^2$ outputs to produce the combined output signal. Figure 2 shows six decorrelated outputs together with the other three received branch signals for a system with $N_r = 3$ branches. It is clear that the diversity decorrelator presents a unique diversity system. For example, the variances of the sum signal $(\widehat{s}_i + \widehat{s}_k)$, the difference signal $(j\widehat{s}_k - j\widehat{s}_i)$, and the branch signal $(\widehat{s}_i)$ are different from the variances of the received branch signals.

However, the sum signal and the difference signal bear some amount of correlation, and, therefore, the conjoint signals, which are the decorrelated outputs, are not all mutually independent and do not lead to diversity gains but coding gains.

*2.6. Conventional Combiner Output SNR.* The probability density function (PDF) of the instantaneous branch SNR for independent signals is provided by Akuon and Xu [28].

$$f_{\overline{\gamma}_k}(\gamma_k) = \begin{cases} \dfrac{1}{\overline{\gamma}_k}\exp\left(-\dfrac{\gamma_k}{\overline{\gamma}_k}\right) & (0 \le \gamma_k < \infty) \\ 0, & \text{otherwise} \end{cases}, \tag{13}$$

where $\overline{\gamma}_k = \Omega_k \frac{E_s}{N_{0k}}$.

For a correlated system, an eigen-filter is used to redistribute branch signal powers. As a result, the SNR due to the channel in Equation (12) is given as follows [28]:

$$\overline{\gamma}_{k,s} = \epsilon_k E\{\gamma_k\} = \epsilon_k E\left[\alpha_k{}^2 \frac{E_s}{N_{0k}}\right] = \epsilon_k \overline{\gamma}_{0,c}. \tag{14}$$

Because Equation (12) has $\widehat{h}_k = \sqrt{\epsilon_k}\widehat{Q}_k\widehat{\widehat{h}} = \sqrt{\epsilon_k}h$, where $\overline{\gamma}_{0,c}$ denotes the average SNR of the combiner output. From the above discussion, it is clear that the output SNRs $\left(\widehat{\widehat{\gamma}}_1, \widehat{\widehat{\gamma}}_2, \cdots, \widehat{\widehat{\gamma}}_{N_r}\right)$ of the eigen-filter signal splitter are scaled eigenvalues of the $c^{th}$ combiner average output SNR $\overline{\gamma}_{0,c}$, i.e.,

$$\widehat{\widehat{\gamma}}_{k,c} = \epsilon_k \overline{\gamma}_{0,c}. \tag{15}$$

The mean output SNR of the independent branch signals for MRC, EGC, and SC can also be calculated as $\overline{\gamma}_{0,c} = \sum_{k=1}^{N_r} \widehat{\widehat{\gamma}}_k$. Furthermore, we can derive from Equation (15) that EVD allows the PDF of the branch SNR at the filter output to be presented as follows:

$$f_{\overline{\gamma}_0}(\gamma_k) = \begin{cases} \dfrac{1}{\widehat{\widehat{\gamma}}_{k,c}}\exp\left(-\dfrac{\gamma_k}{\widehat{\widehat{\gamma}}_{k,c}}\right) & (0 \le \gamma_k < \infty) \\ 0, & \text{otherwise} \end{cases}. \tag{16}$$

The PDF of the SNR results in an equivalent correlated system. The gain of the signal mixing is studied for each combining strategy to evaluate the effect of the signal synthesizer.

*2.7. Synthesizer Gains for MRC, EGC, and SC.* In a study by Akuon and Xu [26], the average output SNRs for MRC, EGC, and SC are derived. In the case of MRC, the average SNR obtained at each branch is given as, $\overline{\gamma}_{0,k,MRC} = \overline{\gamma}$; and it is optimal.

The synthesizer generates four outputs for a two-branch system. The variance of the four outputs may be determined, and the average SNR at the EGC output may be stated as follows:

$$\begin{aligned}\overline{\gamma}_{\text{EGC}} &= \frac{N_r([1+\rho] + [1-\rho] + 1 + 1)\overline{\gamma}}{4}\\ &= N_r\overline{\gamma}\end{aligned}, \tag{17}$$

where $\rho$ denotes the coefficient that assesses the similarity of 2 RV such that $0 < \rho < 1$. As a result, the gain from decorrelation for EGC is expressed as follows:

$$\begin{aligned}G_{\overline{\gamma}}(\text{EGC}) &= \frac{N_r\overline{\gamma}}{\left[1 + (N_r - 1)\frac{\pi}{4}\right]\overline{\gamma}}\\ &= \left[\frac{N_r}{1 + (N_r - 1)\frac{\pi}{4}}\right].\end{aligned} \tag{18}$$

In the two-branch system, $N_r = 2$.

From Shannon's theory, the average SNR at the output for conventional SC, $\overline{\gamma}_{\text{SC}}$, is given as follows:

$$\overline{\gamma}_{\mathrm{SC}} = \log_2(N_r). \tag{19}$$

When conjoint signals are used, one of them could be selected, resulting in $\overline{\gamma}_{\mathrm{SC}}$ being:

$$\overline{\gamma}_{\mathrm{SC}} = \log_2(N_r + 1). \tag{20}$$

Therefore, the decorrelation gain for SC is given as follows:

$$G_{\overline{\gamma}}(\mathrm{SC}) = \frac{\log_2(N_r + 1)}{\log_2(N_r)}. \tag{21}$$

*2.8. New Combiner Output SNR.* Because the new system incorporates a diversity synthesizer, as well as an eigen-filter, we must replace each $\widehat{\widehat{\gamma}}_{k,c}$ with the expression containing the received average branch SNR, $\overline{\gamma}$. The average output SNR, which is equally split per EGC output branch, can be computed from Equations (15) and (18) and is provided as follows:

$$\begin{aligned}\widehat{\widehat{\gamma}}_{k,\mathrm{EGC}} &= G_{\overline{\gamma}(D,\mathrm{EGC})}\epsilon_k \frac{\overline{\gamma}_{0,\mathrm{EGC}}}{N_r} \\ &= G_{\overline{\gamma}(D,\mathrm{EGC})}\epsilon_k \left(\frac{1 + (N_r - 1)\frac{\pi}{4}}{N_r}\right)\overline{\gamma}.\end{aligned} \tag{22}$$

Similarly, from Equations (15) and (21), the average SNR, which is equally split per SC output branch, is given as $\widehat{\widehat{\gamma}}_{k,\mathrm{SC}} = G_{\gamma(D,\mathrm{SC})}\epsilon_k \frac{\overline{\gamma}_{0,\mathrm{SC}}}{N_r}$, which is written as follows:

$$\widehat{\widehat{\gamma}}_{k,\mathrm{SC}} = G_{\overline{\gamma}(D,\mathrm{SC})}\epsilon_k \left(\sum_{i=1}^{N_r} \frac{1}{i}\right)\overline{\gamma}. \tag{23}$$

By letting

$$\beta_c = \begin{cases} 1 & \text{for MRC} \\ \beta_{\mathrm{EGC}} & \text{for EGC} \\ \beta_{\mathrm{SC}} & \text{for SC} \end{cases} \text{ to be the SNR coefficient, we can write}$$

$$\overline{\gamma}_{0,c} = \beta_c \overline{\gamma}. \tag{24}$$

Clearly, it can be seen that for EGC, $\beta_c = G_{\overline{\gamma}(D,\mathrm{EGC})}\left(\frac{1+(N_r-1)\frac{\pi}{4}}{N_r}\right)$, while for SC, $\beta_c = G_{\overline{\gamma}(D,SC)}\left(\sum_{i=1}^{N_r}\frac{1}{i}\right)$.

## 3. Performance Analysis

The performance of the proposed synthesizer under correlation channels is presented in two steps: for square MQAM and BPSK. The two modulation schemes were chosen to demonstrate that the coding gain achieved remains consistent regardless of the modulation scheme used. The coding gain was determined by comparing the SNR of the output signal from a conventional combiner with that of the output signal from a diversity synthesizer. This shows that the coding gain depends on the average SNR of the combiner's output signal and is not influenced by the specific modulation scheme. Therefore, this framework can be applied to various modulation schemes without affecting the coding gain. However, it's important to note that the coding gain may vary when different combiners and diverse fading channels with different PDFs are utilized.

Second, BPSK modulation is known for its resilience, relying on a 180° phase difference between constellation points. This resilience makes it suitable for challenging channel conditions and fading. In cellular communication systems, BPSK is chosen to transmit critical system information on discrete channels [25–29].

Third, the MQAM scheme is favored for its exceptional spectral efficiency, as it improves transmission rates without requiring additional bandwidth. Therefore, MQAM is highly recommended for future wireless communication systems [25, 29, 30].

*3.1. SER for MQAM under Synthesizer System with Correlation.* In a study by Stuber [33], for coherent square MQAM modulation, the symbol error rate (SER) in the AWGN channel is expressed as follows:

$$\begin{aligned}\mathrm{SER}_{\mathrm{MQAM}} = {} & 4\left(1 - \frac{1}{\sqrt{M}}\right)Q\left(\sqrt{\frac{3E_s}{N_0(M-1)}}\right) \\ & -4\left(1 - \frac{1}{\sqrt{M}}\right)^2 Q^2\left(\sqrt{\frac{3E_s}{N_0(M-1)}}\right),\end{aligned} \tag{25}$$

where $\frac{E_s}{N_0} = \overline{\gamma}$ is symbol energy to noise power density in an AWGN channel that is not experiencing fading.

Taking $a$ to be equal to $(1 - \frac{1}{\sqrt{M}})$ and $b$ to be $(\frac{3}{M-1})$, Equation (25) reduces to:

$$\mathrm{SER}_{\mathrm{MQAM}} = 4aQ\left(\sqrt{b\overline{\gamma}}\right) - 4a^2Q^2\left(\sqrt{b\overline{\gamma}}\right). \tag{26}$$

$Q(\cdot)$ denotes the Gaussian Q-function and is given by Craig's formula for $\theta \geq 0$ as $Q\left(\sqrt{b\gamma}\right) = \frac{1}{\pi}\int_0^{\frac{\pi}{2}} \exp\left(-\frac{b\gamma}{2\sin^2\theta}\right)d\theta$ and $Q^2\left(\sqrt{b\overline{\gamma}}\right) = \frac{1}{\pi}\int_0^{\frac{\pi}{4}} \exp\left(-\frac{b\overline{\gamma}}{2\sin^2\theta}\right)d\theta$ [29, 34, 35].

Solving Equation (26) using the trapezoidal rule results in:

$$\mathrm{SER}_{\mathrm{MQAM}} = \frac{a}{t}\left\{\frac{e^{-b\overline{\gamma}/2}}{2} - \frac{\mathrm{a}e^{-b\overline{\gamma}}}{2} + (1-a)\sum_{i=1}^{t-1} e^{-\frac{b\overline{\gamma}}{S_i}} + \sum_{i=t}^{2t-1} e^{-b\overline{\gamma}/S_i}\right\}, \tag{27}$$

where $t$ is the summation value used in the approximation and $S_i = 2\sin^2\theta_i$ and $\theta_i = (i\pi/4t)$.

Furthermore, considering the MRC system over Rayleigh fading channels with a PDF $f_\gamma(\gamma) = \frac{1}{(N_r-1)!\overline{\gamma}^{N_r}}\gamma^{N_r-1}e^{\frac{\gamma}{\overline{\gamma}}}$ of the received SNR, the average symbol error probability of MQAM in this distribution is given as $P_{\mathrm{MRC}} =$

$E(\mathrm{SER}_{\mathrm{MQAM}}) = \int_0^\infty \mathrm{SER}_{\mathrm{MQAM}} f_\gamma(\gamma) d\gamma$. Subsequently, we can compute the $P_{MRC}$ using the gamma function properties given as follows:

For $n > 0$:

$$\int_0^\infty \gamma^{n-1} e^{-\gamma\lambda} d\gamma = \frac{\Gamma(n)}{\lambda^n}, \text{ for } \lambda > 0; \tag{28}$$

where $\Gamma(n) = (n-1)!$, for $n = 1, 2, 3, \ldots$

Accordingly, for the maximum likelihood (ML) detection case, it can be proved that the average $P_{\mathrm{MRC}}$ is given as follows:

$$P_{\mathrm{MRC}} = \frac{a}{t}\left[\frac{1}{2}\prod_{k=1}^{N_r}\frac{2}{b\widehat{\widehat{\gamma}}_{k,c}+2} - \frac{a}{2}\prod_{k=1}^{N_r}\frac{1}{b\widehat{\widehat{\gamma}}_{k,c}+1} + (1-a)\sum_{i=1}^{t-1}\prod_{k=1}^{N_r}\frac{S_i}{b\widehat{\widehat{\gamma}}_{k,c}+S_i} + \sum_{i=t}^{2t-1}\prod_{k=1}^{N_r}\frac{S_i}{b\widehat{\widehat{\gamma}}_{k,c}+S_i}\right]. \tag{29}$$

Finally, by substituting the new values for average branch SNR into Equation (29) using Equations (15) and (24), the general expression for $P_{\mathrm{SER}}$ is given as follows:

$$P_{\mathrm{ser}} = \frac{a}{t}\left[\frac{1}{2}\prod_{k=1}^{N_r}\frac{2}{b\epsilon_k\beta_c\overline{\gamma}+2} - \frac{a}{2}\prod_{k=1}^{N_r}\frac{1}{b\epsilon_k\beta_c\overline{\gamma}+1} + (1-a)\sum_{i=1}^{t-1}\prod_{k=1}^{N_r}\frac{S_i}{b\epsilon_k\beta_c\overline{\gamma}+S_i} + \sum_{i=t}^{2t-1}\prod_{k=1}^{N_r}\frac{S_i}{b\epsilon_k\beta_c\overline{\gamma}+S_i}\right], \tag{30}$$

where $\overline{\gamma}$ is the average received SNR of each branch.

*3.2. SER for BPSK under Synthesizer System with Correlation.* The SER of BPSK in the AWGN channel is expressed as follows [30]:

$$\mathrm{SER}_{\mathrm{BPSK}} = Q\left(\sqrt{b\overline{\gamma}}\right), \tag{31}$$

where $b = 2$ and $Q(\cdot)$ is the Marcum Q-function and it is given by Craig's formula [30].

Following a similar analysis to the MQAM, the SER under correlation and diversity synthesizer is given as follows:

$$P_{\mathrm{SER}} = \frac{1}{4t}\prod_{k=1}^{N_r}\left(\frac{2}{b\beta_c\epsilon_k\overline{\gamma}+2}\right) + \frac{1}{2t}\sum_{i=1}^{t-1}\prod_{k=1}^{N_r}\left(\frac{S_i}{b\beta_c\epsilon_k\overline{\gamma}+S_i}\right). \tag{32}$$

## 4. Discussions and Simulation Results

Monte Carlo simulations are utilized in this section to show the achievable decorrelation gains using the diversity decorrelator. Furthermore, we test the decorrelator's performance for several antenna setups for both MQAM and BPSK modulation schemes. The SER was used to measure performance. In the legend of the figures, the terms "Corr" and "Decorr" refer to the correlated system and the proposed decorrelated system, respectively. "Sim" refers to simulation results, "theory" refers to the results obtained from the analytical framework, and "VRD" is virtual receiver diversity. Further, Rx2, Rx3, and Rx4 are the 2, 3, and 4 diversity orders of received signals, respectively.

The path that connects the transmitter and the receiver is considered to be arbitrarily correlated. In this paper, correlated channels are modeled by the well-known Bessel model. Correlation matrices in correlation models may yield nonpositive semidefinite results [29, 36]. Therefore, it's crucial to assess the validity of each model. There are three primary models: the basic uniform correlation model, the exponential correlation model, and the Bessel correlation model. In large antenna array designs, the uniform correlation model may prove impractical. Instead, exponential and Bessel correlation models are often employed. Interestingly, in both cases, as the number of antennas increases, the performance of diversity gain improves. Additionally, akin to the exponential correlation, the Bessel correlation matrix also exhibits positive semidefinite properties.

In contrast to exponential correlation, which is versatile and can depict correlation in dense or sparse scattering scenarios by adjusting the decorrelation distance, Bessel correlation is suitable only for densely scattered environments [36]. Bessel correlation leads to a greater reduction in diversity gain compared to exponential correlation. Furthermore, exponential correlation results in a less correlated correlation matrix, resulting in more independent antenna numbers compared to Bessel correlation.

Despite its inherent constraints, just like any other model, Bessel correlation can be readily derived through an examination of spatial correlation within a two-dimensional (2D) uniformly distributed configuration, as opposed to a three-dimensional (3D) isotropic scattering context [36]. Furthermore, this inquiry introduces a more plausible

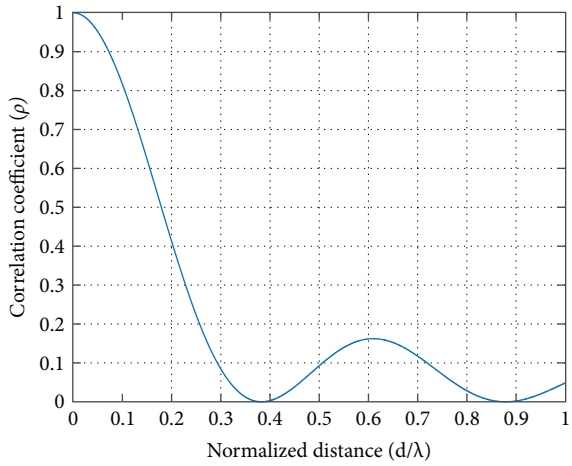


Figure 3: The relationship between correlation and normalized spacing distance.

Table 1: Simulation parameters.

| $\rho = J_0\left(2\pi\frac{N_r d}{\lambda}\right)$ | $J_0\left(2\pi\frac{d}{\lambda}\right)$ | $J_0\left(2\pi\frac{2d}{\lambda}\right)$ | $J_0\left(2\pi\frac{3d}{\lambda}\right)$ | $J_0\left(2\pi\frac{4d}{\lambda}\right)$ |
|---|---|---|---|---|
| $d = 0.1\lambda$ | 0.9037 | 0.6425 | 0.2906 | −0.0550 |
| $d = 0.2\lambda$ | 0.6425 | −0.0550 | −0.4020 | −0.1689 |
| $d = 0.5\lambda$ | −0.3042 | 0.2203 | −0.1812 | 0.1575 |

correlation model, illustrated by the Bessel function of the first kind with a zeroth order, thereby providing a rationale for its favorability within this investigation.

A linear array of antennas with a uniform angle of arrival (AoA) distribution is considered in the correlation model. The correlation coefficient, $\rho$, is expressed as follows [26, 36]:

$$\rho = J_0\left(2\pi\frac{d}{\lambda}\right), \tag{33}$$

where $J_0$ is the zero-order Bessel function, $d$ is the antenna separation distance, and $\lambda$ is the carrier wavelength.

In this study, the choice of antenna spacing was made carefully to keep it below half of the signal wavelength $(\lambda/2)$. When antennas are spaced more than $\lambda/2$ apart, it reduces the correlation between received signals, making them statistically independent. Conversely, closely spaced antennas have a higher correlation coefficient. To accommodate spatial constraints and practical considerations, the antenna spacing was intentionally set to 0.1, 0.2, and 0.5 times the signal wavelength $(\lambda)$. This specific sample size was deemed suitable for our research objectives. The correlation coefficient values range from 0 to 1 $(0 \le \rho < 1)$, and this relationship can be visualized,as shown in Figure 3, using the correlation coefficient equation $\rho = J_o^2(2\pi nd/\lambda)$ and by plotting $\rho$ against the normalized spacing distance, $d/\lambda$.

Using Equation (33), the simulation parameters can be presented, as shown in Table 1.

As a demonstration, choosing an antenna separation distance $d = 0.5\lambda$ and a correlation coefficient $\rho$ while taking

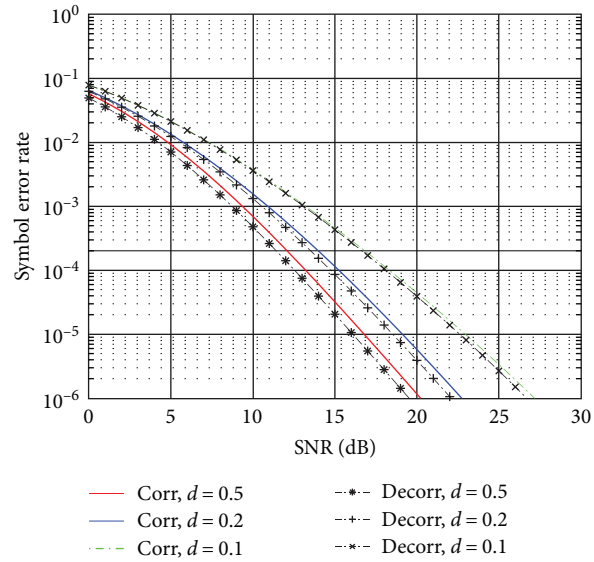


Figure 4: Comparison of simulations for correlated and decorrelated SC SER, where $N_r = 3$.

three equally-spaced receive antennas, $R$, in Equation (8) may be written as follows:

$$R = \begin{pmatrix} 1 & -0.3042 & 0.2203 \\ -0.3042 & 1 & -0.3042 \\ 0.2203 & -0.3042 & 1 \end{pmatrix}. \tag{34}$$

We further note that the number of iterations, $t$, used in Equation (27) was set at $(t = 10)$. It was observed that any $(t > 10)$ had a negligible effect on the accuracy of the results, and this reason informed how the value of $t$ was decided.

*4.1. Discussions under BPSK.* As shown in Figures 4 and 5, we demonstrate the performance of the diversity decorrelator by comparing it with a correlated system. We consider the simulation results for $N_r = 3$ while varying the antenna spacing. As is expected, the more closely spaced antennas experience higher levels of signal correlation, resulting in a higher SER. This is confirmed by the simulation results, which show that the SER decreases from the configuration with $d = 0.1\lambda$ to that of $d = 0.5\lambda$. This occurs because, as the channel conditions deteriorate, closely spaced antennas are more prone to encountering similar fading or interference patterns at the same time. Consequently, the likelihood of experiencing a higher SER increases due to diminished diversity gain, leading to errors manifesting simultaneously across all antennas. The same observations made for the SC system, as shown in Figure 4, are also observed for the EGC system, as shown in Figure 5. More importantly, we note that the proposed diversity decorrelator achieves decorrelation gains of about 1 dB for both the SC and EGC combiner systems at an SER of $10^{-5}$. This is because the sum signal and the difference signal produced from the received signals create combined signals that are virtual, leading to the attainment of coding gains due to increased diversity.

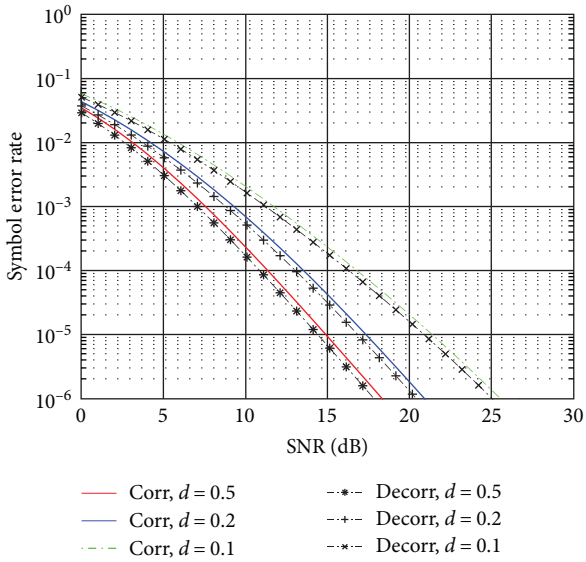


Figure 5: Comparison of simulations for correlated and decorrelated EGC SER, where $N_r = 3$.

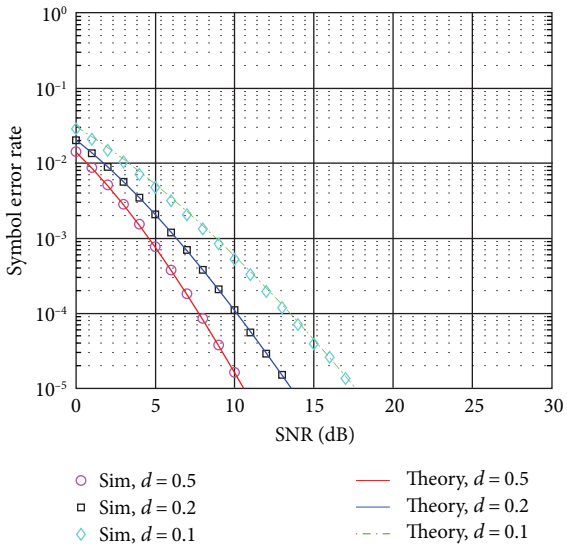


Figure 6: Comparison of decorrelated simulations with theory for EGC SER, where $N_r = 4$.

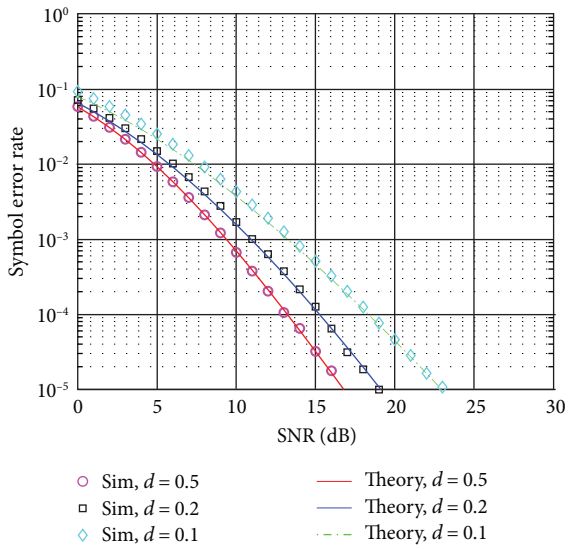


Figure 7: Comparison of decorrelated simulations with theory for SC SER, where $N_r = 3$.

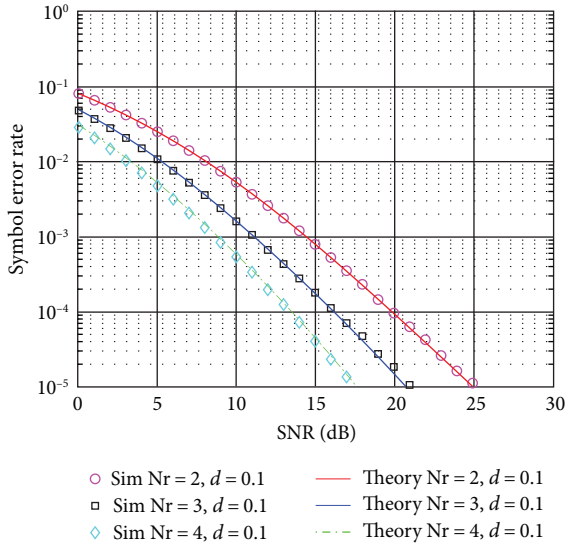


Figure 8: Comparison of decorrelated simulations with theory for EGC SER, where $N_r = 2, 3, 4$, $d = 0.1\lambda$.

Figure 6 shows the simulated results with the analytical model that uses a constant decorrelation gain for the EGC. The proposed decorrelation gain successfully validates the system's response under diversity decorrelation for the EGC combining. The results show that there are close bounds for all tested antenna configurations of $d = 0.1\lambda$, $0.2\lambda$, and $0.5\lambda$, but the analytical approximation method deviates slightly from the simulations due to approximation errors.

As shown in Figure 7, simulated results are compared with the analytical model that uses the proposed analysis for the decorrelation gain of the SC. The proposed decorrelation gain validates the system's response under diversity decorrelation for the SC and shows close bounds for all tested antenna configurations of $d = 0.1\lambda, 0.2\lambda,$ and $0.5\lambda$.

Furthermore, Figures 6 and 7 demonstrate that closely spaced receive branches can lead to a higher correlation between received symbols and potentially a higher SER. Conversely, well-separated branches are more likely to yield a lower SER due to reduced correlation between received symbols and a decreased likelihood of interfering with each other.

Further, simulation tests are conducted to verify the accuracy of the proposed analytical model for different receive diversity branches. Specifically, as shown in Figures 8

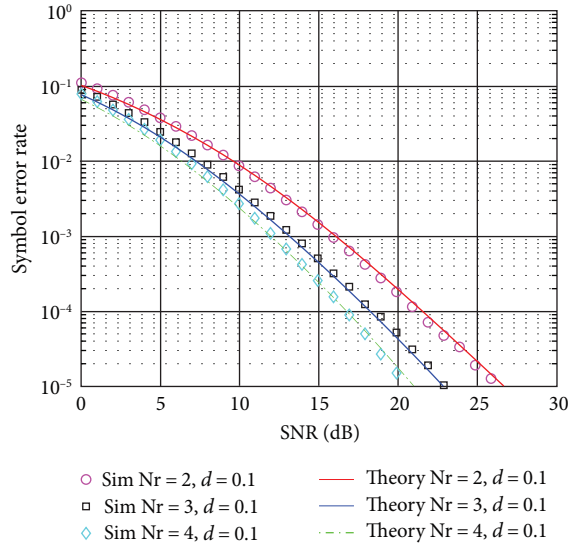


FIGURE 9: Comparison of decorrelated simulations with theory for SC SER, where $N_r = 2, 3, 4, d = 0.1\lambda$.

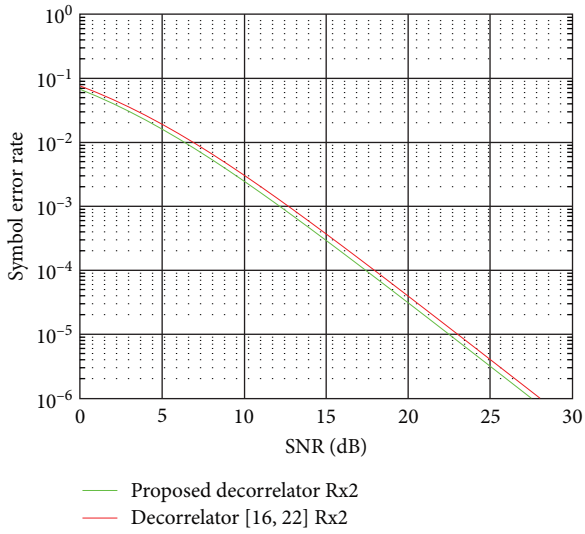


FIGURE 10: Comparison of proposed decorrelator with existing decorrelators, where $N_r = 2$ and $d = 0.1\lambda$.

and 9, the diversity decorrelator systems for EGC and SC are tested for $N_r$ values of 2, 3, and 4. The results show that the analytical model performs well across various diversity branches and closely matches the simulation outcomes. Moreover, the decorrelator's performance improves as the number of receive branches increases. This is because initially, as you add more receiver antennas, the system's diversity gain tends to increase. With more antennas, the system can receive multiple copies of the same signal, each affected by different fading conditions. When these signals are combined, they can help mitigate the effects of fading and improve signal reliability.

Figure 10 shows a comparison between the proposed decorrelator and the decorrelator used in a study by Al-Juboori and Fernando [15] and Hangani and Beaulieu [21]. A correlated system for EGC over BPSK with $d = 0.2\lambda$ and $N_r = 2$ was considered, and SER was used to measure performance. As documented in a study by Al-Juboori and Fernando [15] and Hangani and Beaulieu [21], the application of decorrelation to the dual EGC diversity branches did not yield any discernible improvement in terms of SER and SNR. However, as shown in Figure 10, notable decorrelation gains of ~1 dB were attained at an SER of $10^{-5}$ through the utilization of the proposed decorrelator. Furthermore, it is worth noting that the proposed decorrelator does not impose any restrictions on the number of correlated fading branches, thereby offering enhanced adaptability. In order to evaluate the extent of decorrelation gain, we conducted an analysis of the SNR, both at the output of the combiner as specified in a study by Hangani and Beaulieu [21] and at the output of the newly introduced decorrelator. We integrated Equation (17) from this present study into the SER expression. Importantly, these decorrelation gains, being derived from the SNR expression, remain invariant with respect to the modulation scheme employed, ensuring consistency across various modulation schemes, including MQAM.

*4.1.1. Complexity Analysis.* In a study by Al-Juboori and Fernando [15] and Hangani and Beaulieu [21], a decorrelator is employed with inputs represented as $x_1 = r_1 s + n_1$ and $x_2 = r_2 s + n_2$. These inputs encompass signal samples(s), complex channel, $r_i = \propto_i e^{j\Psi_i}$, for i $\epsilon$ 1, 2, characterized by its amplitude $\propto_i$ and phase $\Psi_i$, while $n_i$ signifies the presence of additive white Gaussian noise (AWGN) for i $\epsilon$ 1, 2. The outputs of the decorrelator are given by $U_1 = \frac{x_1+x_2}{\sqrt{2}} = \frac{r_1+r_2}{\sqrt{2}} s + \frac{n_1+n_2}{\sqrt{2}}$ and $U_2 = \frac{x_1-x_2}{\sqrt{2}} = \frac{r_1-r_2}{\sqrt{2}} s + \frac{n_1-n_2}{\sqrt{2}}$. The decorrelator's complexity analysis is given as follows:

(1) Complex multiplication for $r_1$ and $r_2$: For every complex multiplication, four real multiplications and two real additions are involved, amounting to six operations.
(2) Complex addition for $x_1$ and $x_2$: Each needs two real additions, resulting in four operations.
(3) Scaling by $1/\sqrt{2}$ for $U_1$ and $U_2$: Each scaling operation requires one real multiplication, yielding two operations.
(4) Noise complex Addition for $(n_1 + n_2)/\sqrt{2}$ and $(n_1 - n_2)/\sqrt{2}$ for both $U_1$ and $U_2$: Each addition demands two real additions, totaling four operations.

Summing up these operations, the overall complexity of this decorrelator amounts to 16 operations.

In contrast, in the proposed decorrelator for a two-branch receive system with inputs $\widehat{s}_1 = (X_1 + jY_1)s_1 + n_1$ and $\widehat{s}_2 = (X_2 + jY_2)s_2 + n_2$, signal samples $(s_k)$, complex channel $X_k + jY_k = \propto_k e^{j\theta_k}$, for $k \epsilon$ 1, 2, defined by its amplitude $\propto_k$ and phase $\theta_k$, and $n_k$ represents AWGN for k $\epsilon$ 1, 2. The conjoint signal outputs are $\widehat{v}_3 = \frac{1}{\sqrt{2}}(X_1 + jY_1)\widehat{s}_1 + \frac{1}{\sqrt{2}}(X_2 + jY_2)\widehat{s}_2 + \frac{1}{\sqrt{2}}(n_1 + n_2)$ and $\widehat{v}_4 = -j\frac{1}{\sqrt{2}}(X_1 + jY_1)\widehat{s}_1 + j\frac{1}{\sqrt{2}}(X_2 + jY_2)\widehat{s}_2 + \frac{1}{\sqrt{2}}(-jn_1 + jn_2)$, and its complexity analysis is detailed as follows.

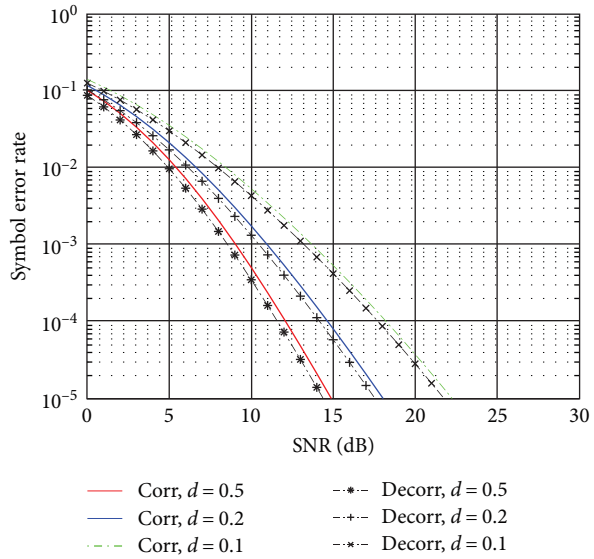


Figure 11: Theoretical and simulated results for EGC with 4 QAM for four correlated and decorrelated branches.

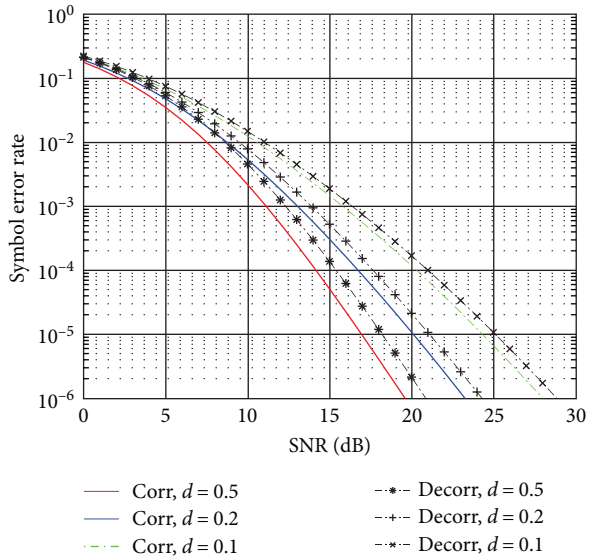


Figure 12: Theoretical and simulated SER results for SC with 4 QAM for four correlated and decorrelated branches.

For each input ($\widehat{s}_1$ and $\widehat{s}_2$), there are two complex additions ($X_1 + jY_1$ and $X_2 + jY_2$), one complex multiplication, and two complex addition with noise ($n_1$ and $n_2$), totaling five operations.

For each output ($\widehat{v}_3$ and $\widehat{v}_4$), there are two complex addition ($X_1 + jY_1$ and $X_2 + jY_2$), one complex multiplication, two scalar multiplication ($1/\sqrt{2}$ or -j/$\sqrt{2}$), and two complex addition with noise ($n_1$ and $n_2$), resulting in seven operations per output.

Considering two inputs and two outputs, the total number of operations for the proposed decorrelator is 24 operations.

When comparing the complexities, the decorrelator in a study by Al-Juboori and Fernando [15] and Hangani and Beaulieu [21] involves 16 operations, whereas the proposed decorrelator entails 24 operations. Therefore, in terms of computational complexity, the decorrelator in a study by Al-Juboori and Fernando [15] and Hangani and Beaulieu [21] is less complex than the proposed decorrelator. That's the trade-off for the additional gain obtained with EGC.

*4.2. Discussions under MQAM.* Figures 11 and 12 show the performance of the virtual diversity decorrelator (VRD) with a correlated system for EGC and SC, respectively, with four receive antennas and spacing of 0.1, 0.2, and 0.5 $\lambda$. As expected, closely spaced antennas with higher signal correlation have a higher SER. The SER decreases as the antenna spacing varies from 0.1 to 0.5 $\lambda$. Above all, the developed decorrelator achieves a coding gain of 0.5 dB for EGC and 1 dB for SC at the SER of $10^{-4}$. This is due to the sum signal and the difference signal generated from the received signals resulting in conjoint signals that are virtual. These conjoint signals result in the coding gains.

Figure 13 shows simulated results from the decorrelator to correlated theoretical results for MRC with diversity orders of 2, 3, and 4 while considering an antenna spacing of 0.5 $\lambda$. The results are in agreement with a study by Dong

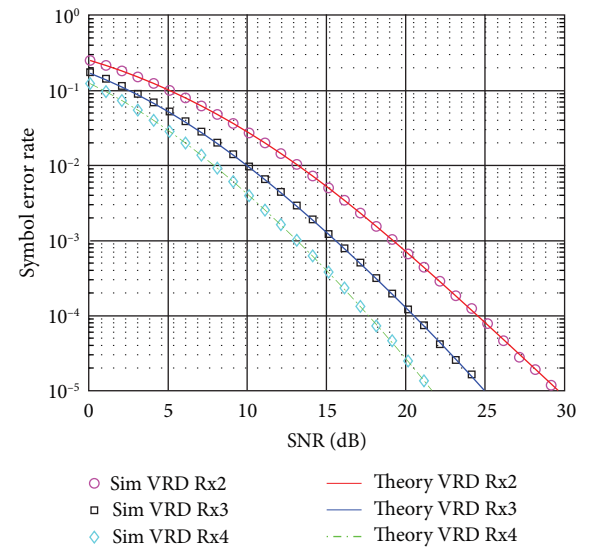


Figure 13: Theoretical and simulated SER results for MRC with 4 QAM for four correlated and decorrelated branches, respectively.

and Beaulieu [22], where the authors concluded that the optimal performance of MRC can be achieved in a diversity system without decorrelating the correlated input branches by selecting the weights of the input branch signals as if they were uncorrelated. More importantly, as shown by Figure 13, the SER decreases as the diversity order increases. As the diversity order increases, more independent copies of the signal become available for combining at the receiver. This, in turn, leads to a higher probability of receiving at least one good copy of the signal, even if some of the branches experience deep fades.

Figures 14 and 15 show the simulated and theoretical results for the decorrelator with 2, 3, and 4 receive antennas while considering an antenna spacing of 0.1 $\lambda$. It can be seen

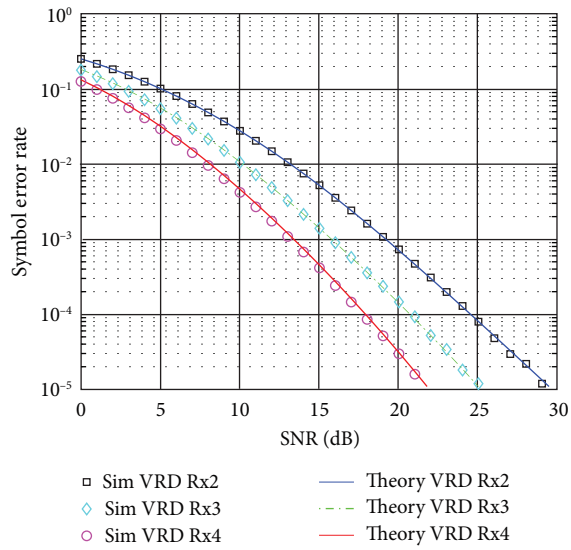


FIGURE 14: Theoretical and simulated SER results for EGC with 4 QAM for decorrelated branches $N_r = 2, 3, 4; d = 0.1\lambda$.

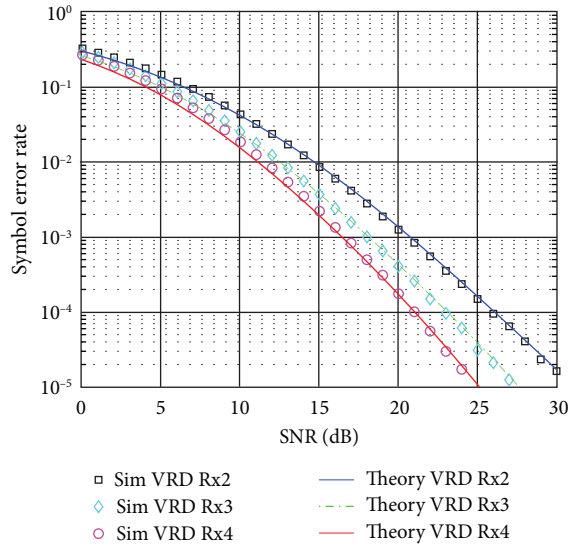


FIGURE 15: Theoretical and simulated SER results for SC with 4 QAM for decorrelated branches $N_r = 2, 3, 4; d = 0.1\lambda$.

that both the simulation and theoretical results match, and the SER decreases as the diversity order increases. This is because, as the diversity order increases, the likelihood of all branches simultaneously experiencing severe fades diminishes. When employing combining methods that utilize multiple signal replicas, the probability of errors caused by fading decreases. This reduction in error probability results in a lower SER and improved overall performance.

Figure 16 shows the square M-QAMs for 4-QAM, 16-QAM, and 64-QAM modulations with a diversity order of 3 and an antenna separation distance of $0.1\lambda$. 4-QAM has better performance followed by 16-QAM, while 64-QAM has the worst performance of the three in terms of SER. This is consistent with the well-known fact that lower-order

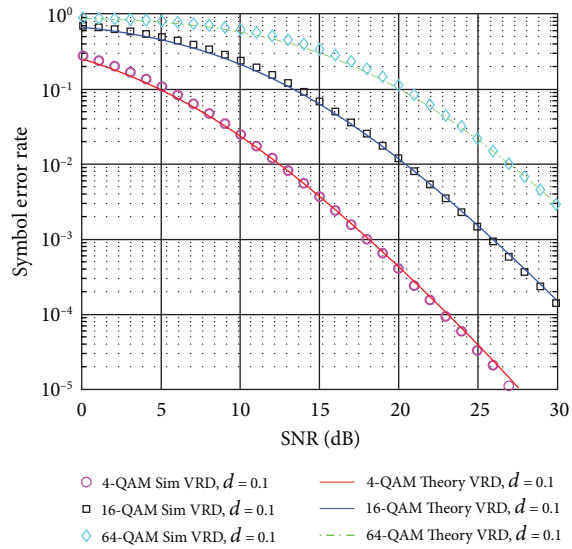


FIGURE 16: Theoretical and simulated SER results for SC with MQAM for three decorrelated branches.

constellations have a lower SER compared to higher-order constellations because for the same mean energy of the constellation, the points are far apart and, hence, less susceptible to noise.

Finally, the introduction of virtual antennas bestows a heightened degree of flexibility upon antenna configurations, eliminating the need for intricate hardware or signal processing mechanisms. This transformative capability leads to a reduction in system complexity and hardware expenditures, as it eliminates the requirement for additional antenna elements to be incorporated at the receiver. However, the application of a virtual diversity synthesizer within the W-band, spanning the electromagnetic spectrum from 75 to 110 GHz, faces several challenges [2, 13, 14]. First, the absence of readily available wideband omnidirectional antennas tailored for frequencies exceeding the 60-GHz threshold in commercial offerings. Second, the assumption of channel uniformity, characterized by identical amplitudes at a phase angle of 45°, while convenient for theoretical analysis, diverges significantly from the realities of practical scenarios where phase angles exhibit variability. Third, there is a need for the deployment of sophisticated signal processing techniques to foster effective collaboration among networked devices. This mandate requires the formulation of innovative algorithms and protocols, as well as the seamless integration of these technological advances into wireless communication frameworks. Finally, although the implementation of the decorrelator serves to reduce signal correlation, it does not achieve complete independence among signals.

## 5. Conclusion

A diversity decorrelator has been presented that achieves decorrelation gains for SC and EGC without the need to measure signal information in a correlated system. From the decorrelated EGC expression in Equation (17), the EGC provides equal error efficiency as the MRC. Unified

SER expressions for MRC, EGC, and SC reception of BPSK and MQAM correlated signals over Rayleigh fading channels have been derived and validated through simulation results.

## Data Availability

The data utilized to support the research findings in this paper are freely available and can be generated using Monte Carlo simulations. The data can also be obtained from the corresponding author upon request.

## Conflicts of Interest

The authors of this research paper have no financial or personal conflicts of interest that could influence the research findings or interpretations during publication.

## Acknowledgments

This research was partially funded by the African Development Bank (AfDB) through the Kenya Ministry of Education.

## References

[1] F. A. García, H. C. Mora, and N. O. Garzón, "Improved exact evaluation of equal-gain diversity receivers in Rayleigh fading channels," *IEEE Access*, vol. 10, pp. 26974–26984, 2022.

[2] H. Al-Anbagi and I. Vertat, "Collaborative network of ground stations with a virtual platform to perform diversity combining," in *2022 International Conference on Applied Electronics (AE)*, 2022.

[3] A. Olutayo, J. Cheng, and J. F. Holzman, "Performance bounds for diversity receptions over a new fading model with arbitrary branch correlation," *EURASIP Journal on Wireless Communications and Networking*, vol. 2020, no. 1, pp. 1–6, 2020.

[4] F. Adachia and A. Boonkajay, "Analysis of maximal-ratio transmit and combining spatial diversity," *IEICE Communications Express*, vol. 8, no. 5, pp. 153–159, 2019.

[5] D. G. Brennan, "Linear diversity combining techniques," in *Proceedings of the IRE*, vol. 47, pp. 1075–1102, 1959.

[6] F. J. Altman and W. Sichak, "A simplified diversity communication system for beyond-the-horizon links," *IRE Transactions on Communications Systems*, vol. 4, no. 1, pp. 50–55, 1956.

[7] R. G. Vaughan and J. B. Andersen, "Antenna diversity in mobile communications," *IEEE Transactions on Vehicular Technology*, vol. 36, no. 4, pp. 149–172, 1987.

[8] L. Khan, "Ratio squarer," in *Proceedings of the IRE*, vol. 42, p. 1704, 1954.

[9] O. O. Ayeni, J. S. Ojo, P. A. Owolawi, and M. O. Ajewole, "Performance comparison of diversity techniques with Addictive White Gaussian Channel (AWGC) in free space optical communication (FSO) under atmospheric turbulence scenario," *International Journal of Physical Sciences*, vol. 18, no. 1, pp. 12–18, 2023.

[10] J. Lin and H. V. Poor, "Optimum combiner for spatially correlated Nakagami-m fading channels," *IEEE Transactions on Wireless Communications*, vol. 20, no. 2, pp. 771–784, 2021.

[11] K. N. Le, "A review of selection combining receivers over correlated Rician fading," *Digital Signal Processing*, vol. 88, pp. 1–22, 2019.

[12] M. Li, F. Zhang, Y. Ji, and W. Fan, "Virtual antenna array with directional antennas for millimeter-wave channel characterization," *IEEE Transactions on Antennas and Propagation*, vol. 70, no. 8, pp. 6992–7003, 2022.

[13] M. Alibakhshikenari, B. Virdee, D. Mariyanayagam et al., "Virtual antenna array for reduced energy per bit transmission at Sub-5 GHz mobile wireless communication systems," *Alexandria Engineering Journal*, vol. 71, pp. 439–450, 2023.

[14] Y. Wang, X. Chen, X. Liu et al., "Improvement of diversity and capacity of MIMO system using scatterer array," *IEEE Transactions on Antennas and Propagation*, vol. 70, no. 1, pp. 789–794, 2022.

[15] S. Al-Juboori and X. Fernando, "Characterizing a decorrelator for selection combining receivers in Nakagami-m fading channels," *AEU—International Journal of Electronics and Communications*, vol. 106, pp. 12–19, 2019.

[16] F. Adachi and R. Takahashi, "On Understanding of optimal joint transmit-receive diversity from eigenmode beamforming in correlated fading channels," in *26th IEEE Asia-Pacific Conference on Communications (APCC), Kuala Lumpur, Malaysia*, November 2021.

[17] F. Zhang, K.-H. Ngo, S. Yang, and A. Nosratinia, "Transmit correlation diversity: generalization, new techniques, and improved bounds," *IEEE Transactions on Information Theory*, vol. 68, no. 6, pp. 3841–3869, 2022.

[18] E. Aksoy, *Advances in Array Optimization*, IntechOpen, London, UK, 2020.

[19] L. Fang, G. Bi, and A. C. Kot, "New method of performance analysis for diversity reception with correlated Rayleigh-fading signals," *IEEE Transactions on Vehicular Technology*, vol. 49, no. 5, pp. 1807–1812, 2000.

[20] S. Loyka, C. Tellambura, A. Kouki, A. Annamalai, and F. Gagnon, "Comments on new method of performance analysis for diversity reception with correlated Rayleigh-fading signals," *IEEE Transactions on Vehicular Technology*, vol. 52, no. 3, pp. 725-726, 2003.

[21] S. Hangani and N. C. Beaulieu, "On the benefits of decorrelation in dual-branch diversity," in *ICC'08*, pp. 4696–4702, 2008.

[22] X. Dong and N. C. Beaulieu, "Optimal maximal ratio combining with correlated diversity branches," *IEEE Communications Letters*, vol. 6, no. 1, pp. 22–24, 2002.

[23] P. J. Schreirer, "A unifying discussion of correlation analysis for complex random vectors," *IEEE Transactions on Signal Processing*, vol. 56, no. 4, pp. 1327–1336, 2008.

[24] M. Tsai, M. Bashir, and M. Alouini, "Data combining schemes for a detector array receiver in free-space optical communications," *IEEE Open Journal of the Communications Society*, vol. 3, pp. 1090–1102, 2022.

[25] W. C. Jakes, *Microwave Mobile Communication*, IEEE Press, New York, 1993.

[26] P. O. Akuon and H. Xu, "Optimal error analysis of receive diversity schemes on arbitrarily correlated Rayleigh fading channels," *IET Communications*, vol. 10, no. 7, pp. 854–861, 2016.

[27] P. O. Akuon and H. Xu, "A receive decorrelator for a wireless communications system," Patent US20180198512, 2019.

[28] P. O. Akuon and H. Xu, "Gain of spatial diversity with conjoint signals," in *IEEE AFRICON, Cape Town, South Africa*, pp. 110–114, 2017.

[29] M. Simon and M. Alouini, *Digital Communication over Fading Channels*, Wiley, New York, 2nd edition, 2004.

[30] H. Xu, "Symbol error probability for generalized selection combining reception of M-QAM," *South African Institute of Electrical Engineers*, vol. 100, no. 3, pp. 68–71, 2009.

[31] F. C. P. de Barros, F. C. M. de Oliveira, M. L. M. G. de Alcoforado, and W. T. A. Lopes, "Performance of polar codes over generalized correlated fading channels," *Journal of Communication and Information Systems*, vol. 37, no. 1, pp. 1–9, 2022.
[32] Y. Pan, Y. Zhou, W. Liu, and L. Ni, "A generalization of principal component analysis," in *2019 IEEE Symposium Series on Computational Intelligence (SSCI)*, vol. 5, pp. 3604–3611, 2020.
[33] G. L. Stuber, *Principles of Mobile Communications*, Kluwer, Norwell, MA, USA, 1996.
[34] Y. Jia, Z. Wang, J. Yu, and P.-Y. Kam, "A new approach to deriving closed-form bit error probability expressions of MPSK signals," *IEEE Transactions on Communications*, vol. 71, no. 8, pp. 4468–4481, 2023.
[35] L. Rugini, "SEP bounds for MPSK with low SNR," *IEEE Communications Letters*, vol. 24, no. 11, pp. 2473–2477, 2020.
[36] X. Chen, "Antenna correlation and its impact on multi-antenna system," *Progress in Electromagnetics Research B*, vol. 62, pp. 241–253, 2015.